
Exploring Sparsity for Parameter Efficient Fine Tuning Using Wavelets

Ahmet Bilican^{1,2} M. Akın Yılmaz² A. Murat Tekalp¹ R. Gökberk Cinbiş³
¹Dept. of Electrical and Electronics Engineering, Koç University ²Codeway AI Research
³Dept. of Computer Engineering, Middle East Technical University

Abstract

Efficiently adapting large foundation models is critical, especially with tight compute and memory budgets. Parameter-Efficient Fine-Tuning (PEFT) methods such as LoRA offer limited granularity and effectiveness in few-parameter regimes. We propose Wavelet Fine-Tuning (WaveFT), a novel PEFT method that learns highly sparse updates in the *wavelet domain* of residual matrices. WaveFT allows precise control of trainable parameters, offering fine-grained capacity adjustment and excelling with remarkably low parameter count, potentially far fewer than LoRA’s minimum—ideal for extreme parameter-efficient scenarios. Evaluated on personalized text-to-image generation using Stable Diffusion XL as baseline, WaveFT significantly outperforms LoRA and other PEFT methods, especially at low parameter counts; achieving superior subject fidelity, prompt alignment, and image diversity.

Code is available at: https://github.com/Bilican/Sparse_PEFT

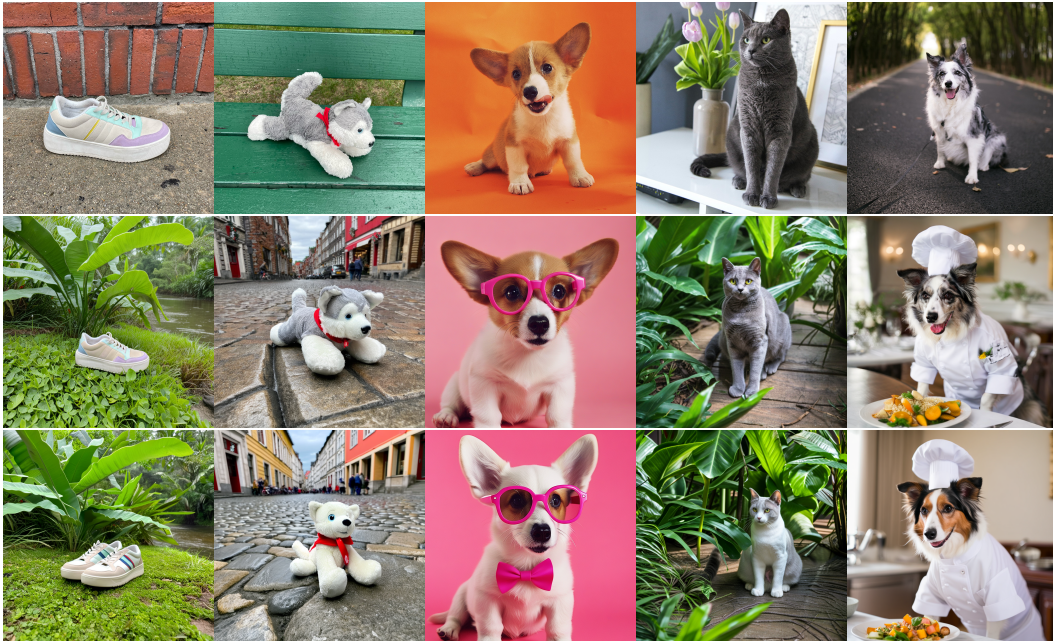


Figure 1: The original images (top), WaveFT results (middle), LoRA results [20] (bottom).

1 Introduction

Large-scale diffusion models, *e.g.* [46, 42], represent the state-of-the-art in text-to-image generation and are increasingly being deployed across industry applications, from mobile features to creative services. Adapting these powerful pre-trained models to specific downstream needs, such as personalizing them to generate images of particular subjects or styles, is crucial for maximizing their utility. However, fully fine-tuning these massive models for each customization [47] is often computationally infeasible due to significant memory requirements, compute costs, and storage needs and can risk degrading the model’s general capabilities through catastrophic forgetting. Parameter-Efficient Fine-Tuning (PEFT) techniques offer a compelling solution by adapting models through training only a small subset of their parameters.

Among PEFT, Low-Rank Adaptation (LoRA) [20] has gained widespread popularity, demonstrating strong performance by learning low-rank updates to the model’s weight matrices. Despite its success, LoRA’s parameter budget is governed by an integer rank $r \geq 1$. In many cases, this lower limit forces allocating more parameters than needed and the discrete increments restrict the granularity of control over the parameter budget over the layers, which potentially hinder PEFT-efficiency.

To this end, we introduce Wavelet-domain Fine-Tuning (WaveFT) that learns a sparse set of parameters, denoted by p , in the *wavelet domain* representation of the weight update matrix ΔW . These learned sparse coefficients are subsequently transformed back to the standard weight domain via the Inverse Discrete Wavelet Transform (IDWT) to yield the final update. To serve as a baseline to demonstrate the effect of the wavelet transform, we provide comparisons to SHiRA [5], which applies sparse updates directly in the weight domain. The proposed sparse parameterization, governed by p , permits much more granular adjustment of the adaptation budget compared to LoRA’s integer rank r , allowing tuning well below the minimum trainable parameter for LoRA (at $r = 1$).

Formulating adaptation as sparse updates within the wavelet domain offers distinct advantages: Wavelet bases excel at representing data with semilocal structure. By learning sparse coefficients in this domain, WaveFT can efficiently model localized yet structured model modifications. This enables better capture of the fine-grained details and instance-specific characteristics essential for high-fidelity personalized image generation, compared to the global nature of low-rank updates.

We present a detailed theoretical analysis which applies to both WaveFT and SHiRA [5] with comparisons to LoRA. We also performed a comprehensive empirical evaluation on the DreamBooth benchmark [47]. Our experimental results show that WaveFT consistently surpasses LoRA and other competitive PEFT baselines when compared at equivalent parameter counts, and support theoretical insights. WaveFT demonstrates superior performance across vital metrics, including subject fidelity (identity preservation), prompt alignment (text following), image diversity, and distributional similarity to real images (CMMD [24]).

In summary, our main contributions are: (i) WaveFT, a novel PEFT method that introduces trainable sparse parameters in the wavelet domain, offering fine-grained control over the parameter budget and leveraging wavelet properties for efficient model adaptation; (ii) Theoretical analysis of a category of sparse fine-tuning methods including WaveFT and SHiRA [5]. (iii) extensive experiments on personalized generation demonstrating that WaveFT achieves state-of-the-art results compared to existing PEFT methods [20, 52, 29, 57]; (iv) in-depth ablation studies validating WaveFT’s design choices and offer complementary insights into its distinct advantages.

2 Related Work

PEFT and intrinsic dimensionality. The feasibility of PEFT is partly motivated by the concept of *intrinsic dimensionality*, suggesting that the essential changes required for downstream tasks might reside in a low-dimensional subspace [30, 1]. Aghajanyan et al. [1] specifically showed that fine-tuning large language models (LLMs) effectively occurs within low-dimensional subspaces. While some methods explicitly combine low-rank and sparse updates [40, 22, 55], others directly fine-tune only specific components, such as biases or partial connections [51].

LoRA extensions. LoRA [20] is perhaps the most prominent PEFT method, achieving efficiency by representing the weight update ΔW as a product of two low-rank matrices, $\Delta W = BA$. This low-rank constraint significantly reduces trainable parameters, controlled by the rank r . Numerous

extensions have been proposed to improve LoRA. Some focus on dynamically allocating the parameter budget (rank) based on layer importance [57, 25, 61] rather than using a fixed rank. Others explore alternative matrix factorizations involving Hadamard or Kronecker products [23, 52, 7, 11]. Significant effort has also gone into improving parameter efficiency further through shared parameter schemes [29, 31, 26, 10], multi-scale structures [60], summation compression [44], or optimizing shared and specific modules [39, 56]. Other works delve into the internal mechanics, analyzing the asymmetry of LoRA matrices [62], decomposing weights differently [34], optimizing training dynamics [17, 32, 48], or using weight guidance [27]. While these methods enhance LoRA, they typically retain the core low-rank decomposition and the limitation of discrete rank control. Our approach fundamentally differs by using direct sparsity parameterization (p) instead of rank (r), allowing finer budget control.

Transformed parameterizations. Several recent methods explore adapting models by operating in domains other than the standard weight space. FourierFT [15] learn sparse updates in the 2D discrete Fourier domain, while FouRA [6] applies 1D Fourier transforms to embeddings before LoRA. The proposed WaveFT shares the spirit of operating in a transformed domain but specifically utilizes the wavelet domain. Other related directions include methods that directly adapt components derived from Singular Value Decomposition (SVD) of weights, such as singular values or vectors [53, 12, 19, 4], use deconvolution in subspaces [54], or constraining the fine-tuning updates to be orthogonal transformations [43, 35, 37].

Sparse Fine-Tuning. Sparse fine-tuning methods update only a small, fixed subset of model weights to achieve parameter-efficient adaptation. Earlier work includes DiffPruning [16], Fisher Mask [49], LT-SFT and Composable SFT [2], which use various masking strategies to select individual weights. Recent approaches like SpIEL iteratively grow and prune indices [3], SMT partitions weights into blocks for gradient-based selection [18], SHiRA explores various types of sparse masks and demonstrates: (a) significantly better performance than LoRA, and (b) reduced concept loss in multi-adapter usecases [5], and SaRA identifies low-magnitude weights for progressive sparse adaptation [21].

As direct relevant baselines, we include *SHiRA-rand* in [5] (we refer to as SHiRA for brevity) learning random sparse updates in the weight domain, and FourierFT [15], which selects trainable parameters uniformly at random in the fourier domain.

Finally, we note that while many PEFT methods demonstrate success primarily on NLP tasks, their effectiveness and characteristics can differ in the vision domain [52]. Our work provides a thorough evaluation of sparse adaptation methods (SHiRA, WaveFT) in the challenging context of text-to-image personalization, with comparisons against strong low-rank and structured PEFT baselines.

3 Sparse Fine-Tuning in the Wavelet Domain

Large pre-trained models are adapted by adding a small update matrix ΔW to the original parameters $W_0 \in \mathbb{R}^{m \times n}$ with weight λ , such that

$$W = W_0 + \lambda \Delta W.$$

In the case of LoRA, ΔW_{LoRA} is constrained to be a low-rank matrix. Our proposed method instead focuses on learning ΔW with a sparse parameterization in a way that allows controlling the number of trainable parameters in a fine-grained manner.

WaveFT is our primary proposed method, which learns a sparse set of parameters within the *wavelet domain* representation of the weight update matrix. More specifically, the update ΔW_{WaveFT} is obtained by applying the 2-Dimensional Inverse Discrete Wavelet Transform (IDWT) to a sparse coefficient matrix $C \in \mathbb{R}^{m \times n}$:

$$\Delta W_{\text{WaveFT}} = \text{IDWT}(C)$$

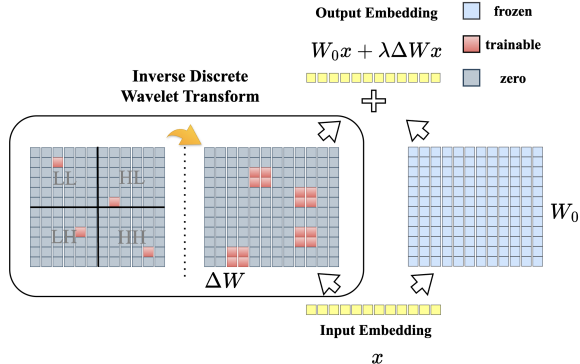


Figure 2: Overview of the proposed method.

The matrix C contains the trainable parameters in the wavelet domain. It is constructed to be sparse: C is initialized as a zero matrix ($\mathbf{0}$), ensuring $W = W_0$ at the start of training. We investigate alternative initializations, such as sampling the p trainable parameters from a Gaussian distribution, in our experiments (Section 5). We then select exactly p entries of C uniformly at random to serve as trainable parameters. The number of trainable parameters per layer, p , is chosen for parameter efficiency (e.g., to match LoRA $r = 1$ or be even smaller). In our standard setup, the budget p is fixed for all adapted layers, though adaptive allocation is explored in Section 5. During optimization, gradients are computed only for the p trainable entries in C .

We hypothesize that the structure introduced by the wavelet transform provides an effective parameterization for highly sparse $p \ll m \cdot n$ choices. In our experiments, we thoroughly investigate the validity of this hypothesis with comparisons to unstructured weight-space sparsity, *i.e.* SHiRA [5], or global low-rank approximations, *e.g.* LoRA [20]. We note that SHiRA [5] can be expressed as a special case of WaveFT via replacing IDWT operators in WaveFT by identity mapping.

This approach of selecting p specific entries for training, as in SHiRA [5] and our WaveFT, can be viewed through the lens of intrinsic dimensionality [1]. By fixing all but p randomly chosen elements of ΔW (for SHiRA) or C (for WaveFT) to zero, we effectively restrict the optimization to a p -dimensional subspace of the full $m \times n$ dimensional space, spanned by the standard basis vectors corresponding to these p chosen entries. For WaveFT, a subsequent linear transformation (the IDWT) is then applied to the parameters residing in this sparsely defined subspace.

Inference efficiency. WaveFT provides efficient inference. After training, the learned update ΔW (either $\Delta W_{\text{WaveFT}} = \text{IDWT}(C)$ or $\Delta W_{\text{SHiRA}} = C$) can be computed once and merged with the original weights:

$$W_{\text{final}} = W_0 + \lambda \Delta W$$

Using W_{final} incurs no inference latency overhead compared to the original model W_0 . This ensures that the inference speed after merging the adapter is identical to that of the original pre-trained model.

4 Theoretical Analysis

The empirical results presented in Section 5, specifically Fig. 4 and Table 4 (appendix), demonstrate that sparse methods, WaveFT and SHiRA [5], produce more diverse outputs when generating new images compared to other parameter-efficient fine-tuning techniques like LoRA. This section provides a theoretical framework to help understand this phenomenon. In the following, we present a series of lemmas that collectively build an argument for the enhanced representational capacity of WaveFT and SHiRA [5], which stems from their ability to realize high-rank updates to the model weights. This increased capacity is hypothesized to be the foundation for the observed diversity.

At the core of our analysis is the use of a sparse update matrix. Lemma 1 [14, 13] offers fundamental insight into the rank properties of such matrices when constructed with randomly selected non-zero entries.

Lemma 1. *Let A_n be an $n \times n$ matrix whose entries are initially all zero. Suppose $p = n(\ln n + c_n)$ distinct positions are chosen uniformly at random from the n^2 available positions in A_n . These p chosen positions are then filled with random non-zero values.*

The probability that the resulting matrix A_n is full rank satisfies:

$$\lim_{n \rightarrow \infty} \Pr(A_n \text{ is full rank}) = \begin{cases} 0 & \text{if } c_n \rightarrow -\infty, \\ e^{-2e^{-c}} & \text{if } c_n \rightarrow c, \\ 1 & \text{if } c_n \rightarrow \infty. \end{cases}$$

Lemma 1 provides an asymptotic guarantee: a sufficiently sparse random matrix ΔW (where *sufficiently sparse* implies the number of non-zero elements p is at least $n(\ln n + c_n)$) is highly likely to be full rank as matrix dimensions grow. Given that the probability of an $m \times n$ matrix with p nonzero entries being full rank is higher than $n \times n$ matrix (for $m \geq n$), this Lemma 1 also holds for $m \times n$ matrices. In SHiRA [5], the update ΔW_{SHiRA} is precisely such a sparse matrix, where p entries are randomly chosen to be trainable.

Figure 3 empirically shows the rank of a randomly generated sparse matrix (denoted \hat{r}) versus the number of non-zero elements p for attention layer matrix dimensions in the SDXL model [42]. 95% confi-

dence intervals are shown as shaded. Vertical dashed lines indicate LoRA complexity levels for varying r values according to the corresponding number trainable parameters. The figure demonstrates that the resulting matrix rank rapidly increases as a function of p as asymptotically predicted by Lemma 1 and reaches full rank at a parameter complexity that would correspond to a LoRA adapter with $r = 3$. Thus, we can operate with high confidence that ΔW_{SHiRA} is high-rank.

The WaveFT method, which applies an update $\Delta W_{\text{WaveFT}} = \text{IDWT}(C)$, also begins with a sparse matrix C in the wavelet domain. This matrix C is constructed identically to ΔW_{SHiRA} : p randomly selected coefficients are made trainable, while the rest are zero. The Inverse Discrete Wavelet Transform (IDWT) is a linear transformation that preserves rank. Consequently, the high-rank property established for C (supported by Lemma 1 and Figure 3) directly implies that ΔW_{WaveFT} will also be high-rank.

This inherent characteristic of SHiRA [5] and WaveFT—their tendency to produce high-rank updates—contrasts starkly with methods like LoRA [20], which are explicitly designed to yield low-rank updates. Lemma 2 formalizes this critical difference and its implications.¹

Lemma 2 (Subspace Bottleneck of LoRA). *For a rank- r adapter update matrix of the form $\Delta W = BA^\top$, where $B \in \mathbb{R}^{m \times r}$ and $A \in \mathbb{R}^{n \times r}$, the following properties hold:*

1. *The image (column space) of ΔW is contained within the span of the columns of B :*

$$\text{im}(\Delta W) = \{\Delta W x \mid x \in \mathbb{R}^n\} \subseteq \text{span}(\text{columns of } B).$$

2. *The kernel (null space) of ΔW contains the orthogonal complement of the span of the columns of A :*

$$\ker(\Delta W) = \{x \in \mathbb{R}^n \mid \Delta W x = 0\} \supseteq (\text{span}(\text{columns of } A))^\perp = \ker(A^\top).$$

Consequently, any update ΔW achieved through such a factorization can only modify the network’s activations within the r -dimensional subspace spanned by the columns of B . Directions orthogonal to the columns of A in the input space are mapped to zero.

Lemma 2 clearly illustrates that LoRA [20] constrains the update ΔW to a low-rank structure. As a result, any changes LoRA makes to the model’s behavior are confined to a low-dimensional subspace—specifically, the r -dimensional space spanned by the columns of its B matrix. This *subspace bottleneck* inherently limits the range and complexity of modifications LoRA can represent.

Having established that our methods produce high-rank updates while LoRA [20] is confined to low-rank ones, we now consider the representational power that high-rank sparse matrices offer:

Lemma 3 (Block-Sparse Interpolation Capacity). *Let $W_0 \in \mathbb{R}^{m \times n}$ be any fixed matrix. Let*

$$\{x^{(1)}, \dots, x^{(k)}\} \subset \mathbb{R}^n$$

be linearly independent, and let arbitrary targets $\{y^{(1)}, \dots, y^{(k)}\} \subset \mathbb{R}^m$ be given. Set

$$X = [x^{(1)} \ \dots \ x^{(k)}] \in \mathbb{R}^{n \times k}, \quad Z = [y^{(1)} - W_0 x^{(1)} \ \dots \ y^{(k)} - W_0 x^{(k)}] \in \mathbb{R}^{m \times k}.$$

Let $S \subset [m] \times [n]$ be a fixed sparse support pattern, and define

$$R = \{i \in [m] \mid Z_{i,:} \neq 0\}, \quad S_i = \{j \in [n] \mid (i, j) \in S\}.$$

Assume:

1. $\text{rank}(X) = k$.

¹Proofs are in Section A.4

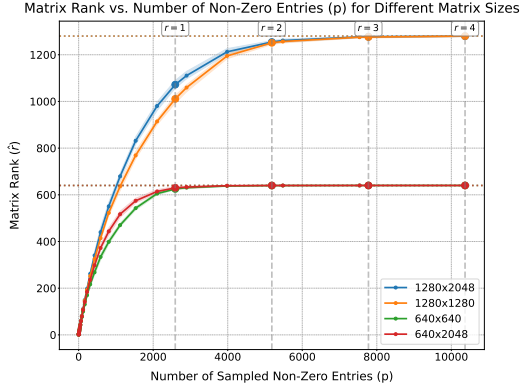


Figure 3: Rank analysis random sparse matrices.

2. There exists a single index set

$$C = \{c_1, \dots, c_k\} \subset [n]$$

such that $X_{C,:} \in \mathbb{R}^{k \times k}$ is invertible and $C \subset S_i$ for every $i \in R$.

Then one can construct $\Delta W \in \mathbb{R}^{m \times n}$ with

1. $\text{supp}(\Delta W) \subseteq S$.
2. $(W_0 + \Delta W)x^{(l)} = y^{(l)}$ for all $l = 1, \dots, k$.
3. $\text{rank}(\Delta W) = \text{rank}(Z_R)$, where Z_R is the submatrix of Z restricted to rows in R .

Lemma 3 provides a powerful insight: if a sparse support pattern S is suitably structured relative to a set of k linearly independent inputs $x^{(l)}$ and desired outputs $y^{(l)}$, then a ΔW confined to this support S can perfectly interpolate these target transformations. Specifically, Hypothesis 2 of the lemma requires that for all rows i where a change is needed (i.e., $i \in R$), the sparse support S_i in that row must contain a common set of k column indices C such that the input submatrix $X_{C,:}$ is invertible. When these conditions hold, an update ΔW can be constructed that not only matches the desired input–output behavior but whose rank is at least that of the necessary change Z_R .

While Lemma 3 considers a fixed support S , our methods utilize randomly generated sparse supports. The connection arises because the high probability of achieving a high-rank update matrix (as established by Lemma 1 and Figure 3 and demonstrated in Section 5.2) implies that the randomly chosen support S is rich enough to allow for the construction of such a ΔW for a substantial number of target transformations. If the desired set of transformations $\{(x^{(l)}, y^{(l)})\}_{l=1}^k$ requires a high-rank Z_R (representing diverse and complex changes), then the resulting ΔW must also be high-rank. Our methods inherently produce such high rank updates, suggesting they possess greater capacity to represent complex, high-dimensional changes.

This theoretical framework explains the increased output diversity observed with our methods. The ability to operate effectively in a much higher-dimensional modification space means SHiRA and WaveFT are not confined by the “subspace bottleneck” of LoRA. They can represent a richer, more varied family of transformations from the base model. When applied to image generation, this expanded representational power allows the fine-tuned model to explore a broader manifold of possible outputs. Rather than being restricted to changes along only r fixed “directions” as in LoRA, our methods can combine learned sparse parameters to produce a wider array of nuanced adjustments. This theoretical capacity to span a larger functional space provides a strong basis for the empirically observed outcome: **WaveFT and SHiRA [5] produce more diverse image generations, as evidenced by the diversity scores in Fig. 4 and Table 4 (appendix).**

5 Experiments

We evaluate WaveFT and SHiRA [5] primarily on personalized text-to-image generation using the SDXL model [42] with the 30 DreamBooth instances [47]. Key metrics include DINO [41] and CLIP-I [45] similarity for subject fidelity, CLIP-T [45] score for prompt alignment, LPIPS [58] for image diversity, and CMMD [24] for distributional similarity to real images. Unless specified otherwise, all methods are configured for a fair comparison with a parameter budget equivalent to LoRA $r = 1$ (≈ 1.451 M trainable parameters for SDXL attention layers). LoRA, WaveFT, and SHiRA [5] all require ≈ 17 GB of memory during training.

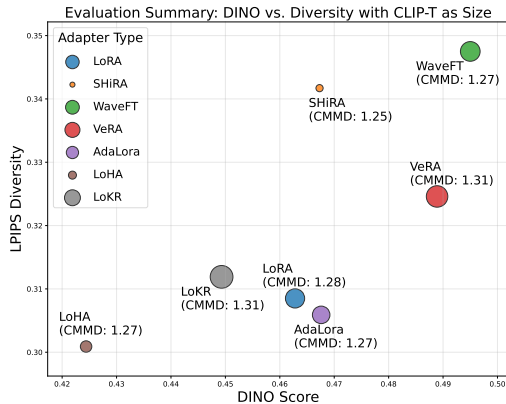


Figure 4: Evaluation of PEFT methods.

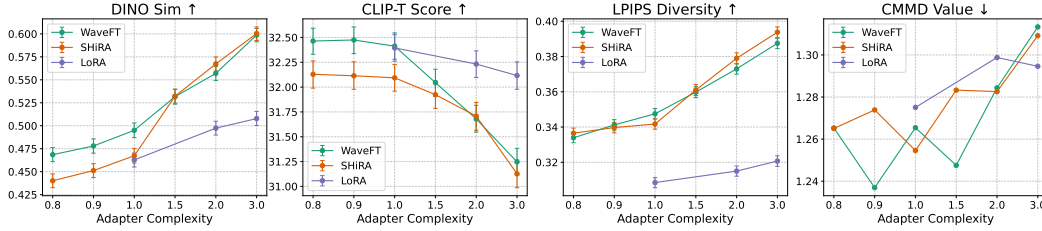


Figure 5: Performance of WaveFT, SHiRA [5], and LoRA [20] across adapter complexity settings, where the unit complexity (1) is defined as the number of trainable parameters corresponding to the LoRA adapter at rank $r = 1$. WaveFT excels at lower parameter counts for subject fidelity (DINO) while maintaining competitive performance elsewhere.

5.1 Personalized Text-to-Image Generation

Figure 4 provides a visual summary of method rankings. WaveFT consistently outperforms other PEFT [38] methods, especially in subject fidelity and image diversity, while maintaining strong prompt adherence. We also see that WaveFT significantly improves upon SHiRA [5], particularly in subject fidelity, highlighting the advantage of learning sparse updates in the wavelet domain. Table 4 (appendix) reports the detailed performance scores on the DreamBooth benchmark.²

WaveFT vs. SHiRA: Impact of Wavelet Domain and Parameter Budget: We further analyze WaveFT against SHiRA across varying parameter budgets (LoRA equivalent ranks 0.8 to 3.0), detailed in Table 2 (appendix) and Figure 5. WaveFT shows a clear subject fidelity advantage (DINO, CLIP-I) at lower budgets. For instance, WaveFT at rank 0.8 surpasses LoRA at rank 1. As parameters increase, SHiRA’s subject fidelity becomes comparable. Figure 5 illustrates this trend for DINO similarity. For prompt fidelity (CLIP-T), WaveFT generally maintains an edge or performs comparably. Increasing the number of parameters for better subject fidelity slightly reduces prompt fidelity for both methods. Image diversity (LPIPS) consistently improves with more parameters for both, with SHiRA often showing a slight edge. CMMD scores show mixed trends. Crucially, these sparse methods allow fine-grained budget control. The results (e.g., WaveFT $p \approx 0.8r$ outperforming LoRA $r = 1$) underscore WaveFT’s parameter efficiency.

Ablation Studies and Design Choices for WaveFT: We validated WaveFT’s default configuration through several ablations.

- **Initialization:** Zero-initialization of the p trainable parameters in the coefficient matrix C proved robust. Gaussian initialization performed drastically worse (Table 3, appendix), confirming our simpler strategy.
- **Wavelet Family:** Various wavelet families (Coiflets, Daubechies, Symlets) yielded strong, comparable performance (Table 1, appendix). The computationally simpler Daubechies 1 (Haar) was chosen as default due to its robust top-tier results (e.g., Symlet 3, Daubechies 2 in Table 3 in appendix show similar performance).
- **Parameter Allocation:** Allocating a fixed p to each layer outperformed allocating parameters proportionally to layer size ($m + n$) for a similar total budget (Table 3).
- **Location Seed Stability:** WaveFT yields more stable and better results than SHiRA due to it being less sensitive to the random selection of p trainable locations across different seeds (Table 5, appendix).
- **Learned Coefficients Analysis:** The energy levels across wavelet subbands (Fig. 9) did not show clear dominance of any subband, supporting our uniform random selection of trainable coefficients.
- **Robustness to Input Permutation:** To test if WaveFT relies on input embedding locality, we permuted input token order to attention layers during training with a random seed and used the same seed in inference. While performance slightly degraded (Table 3 in appendix, “Permuted Input”), WaveFT still significantly outperformed SHiRA [5]. This suggests WaveFT’s advantage is not dependent on the input structure, and the wavelet domain offers a more general sparse parameterization benefit.

²Due to its complete failure, values for FourierFT is not included in Fig. 4 and can be found in Table 4

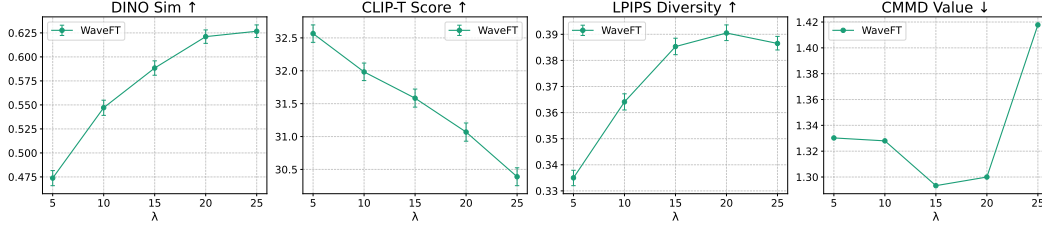


Figure 6: Effect of λ on WaveFT performance (rank-4 equivalent parameters). Increasing λ tends to enhance subject fidelity (DINO, CLIP-I) at the cost of prompt alignment (CLIP-T).

- Zero-padding is applied as needed if matrix dimensions (m, n) are not ideal for standard 2D DWT/IDWT algorithms.

Effect of Output Scaling λ : The output scaling factor λ in $W = W_0 + \lambda\Delta W$ allows tuning the trade-off between subject fidelity and prompt alignment. For WaveFT, increasing $\lambda \in \{5, \dots, 25\}$ generally improved subject fidelity while decreasing prompt alignment (Table 6 in appendix, Figure 6). This provides a controllable mechanism similar to LoRA’s α/r .

5.2 Empirical Demonstration of Block-Sparse Interpolation Capacity

To illustrate the practical implications of Lemma 3, we conduct an experiment involving mapping $k = 5$ random input vectors to $k = 5$ random output vectors. With high probability, the $n \times k$ input matrix X satisfies Hypothesis 1 ($\text{rank}(X) = k$). A crucial condition for interpolation via Lemma 3 is Hypothesis 2: there must exist a k -subset of column indices C (where $X_{C,:}$ is invertible) such that this set C is contained within the support S_i of every row $i \in R$ that requires an update. For this experiment, we set the number of rows $n = |L| = |R| = 784$ and use a total of $m = n\mu = 784 \times 20 = 15,680$ trainable parameters.

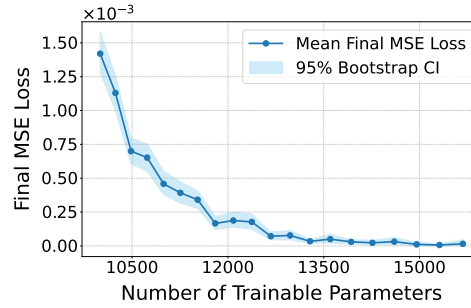


Figure 7: The final loss achieved in training after setting p parameters trainable

To assess whether the row supports S_i are likely to be sufficiently rich to contain such a common set C , we model the number of trainable parameters, X_r , falling into a specific row r . This is described by

$$X_r \sim \text{Binomial}(m, 1/n),$$

which assumes that each of the m trainable parameters is assigned to one of the n rows uniformly and independently. We aim for each relevant row to have at least $k = 5$ trainable parameters, i.e., $X_r \geq k$.

The probability that a given row has fewer than k parameters is

$$P(X_r < k) = \sum_{j=0}^{k-1} \binom{m}{j} \left(\frac{1}{n}\right)^j \left(1 - \frac{1}{n}\right)^{m-j}.$$

Using a union bound, the probability that any of the n rows has $X_r < k$ is

$$P(\exists r : X_r < k) \leq n \cdot P(X_r < k).$$

For $m = 15,680$ and $k = 5$, this probability is ≤ 0.01 .

Therefore, with at least 99% probability, each row’s support S_i contains at least $k = 5$ elements. While this doesn’t strictly guarantee the existence of a common set C across all relevant rows, it makes the conditions of Lemma 3 highly probable when using randomly generated sparse supports. The empirical results shown in Figure 7 align with this: the training loss is zero when $p = m = 15,680$ trainable parameters are utilized.

6 Limitations

MNIST Classification. To demonstrate the potential of WaveFT and SHiRA [5] beyond complex generative models, we applied them as single-layer classifiers on the MNIST dataset[8]. Figure 8 shows that both methods can function as efficient, standalone layers, achieving competitive classification accuracy with a small number of parameters but we see that there in the classification task, SHiRA [5] performs better than WaveFT. This implies that there are different trade-offs for different tasks when changing domain in which sparse paramete

Our work, while demonstrating the strong promise of WaveFT, has some limitations offering avenues for future research.

Hyperparameter tuning. The computational requirements of training and evaluating multiple PEFT methods across 30 personalized instances (100 images for each instance) necessarily constrained the breadth and depth of our hyperparameter search. While we employed established learning rates (e.g., 1×10^{-4}) and common configurations where possible, and our default settings for WaveFT/SHiRA (zero-initialized trainable parameters, $\lambda = 25$) proved effective, an exhaustive hyperparameter search might yield further gains in some cases.

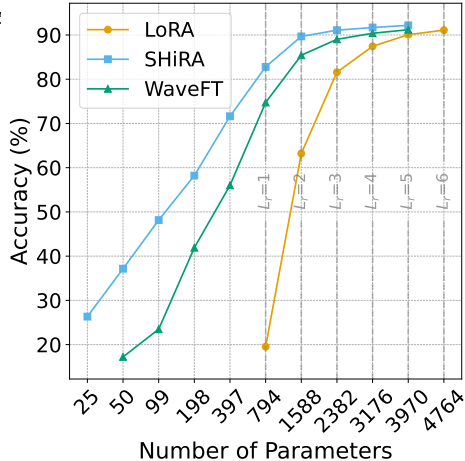


Figure 8: MNIST classification accuracy

Model and task scope. All experiments presented were conducted on the Stable Diffusion XL (SDXL) 1.0 base model. Although SDXL is a prominent and powerful diffusion model, applications of WaveFT and SHiRA to other generative image models is an important future work direction. Similarly, to fully understand the general efficacy of WaveFT, we plan to explore other fine-tuning tasks, such as style adaptation, general domain transfer, controllable generation beyond subject identity, or down-stream tasks in language models.

Sparsity pattern selection. WaveFT selects p trainable parameter locations in C uniformly at random. While our stability analysis showed robustness, this is a simple approach. More sophisticated strategies (e.g. importance-based selection, structured sparsity, learned masks) were not explored and are promising directions for future work.

Further theoretical understanding. Finally, while our work provides strong theoretical and empirical evidence for the effectiveness of WaveFT, a deeper theoretical understanding of how sparse updates in transformed domains interact with the learning dynamics, representation geometry, and inductive biases of large-scale foundation models remains an important area for future investigation.

7 Conclusion

This paper demonstrates that adaptation of a randomly selected sparse subset of weights is a promising parameter-efficient fine tuning (PEFT) approach. We introduce Wavelet Fine-Tuning (WaveFT), a novel PEFT method that learns highly sparse updates in the weight-wavelet domain, offering precise control over trainable parameters. Compared to SHiRA [5], a direct sparse weight-domain baseline, and other established PEFT methods such as LoRA [20], WaveFT demonstrates significant advantages in personalized text-to-image generation with SDXL. Our extensive experiments show WaveFT achieves superior subject fidelity and image diversity while maintaining strong prompt alignment, particularly excelling in low-parameter regimes. This underscores the effectiveness of leveraging the wavelet domain for sparse adaptation. WaveFT offers a potent and highly efficient strategy for adapting large foundation models, paving the way for further exploration into structured sparsity in transformed domains and broader applications.

Acknowledgements. Special thanks to Hasan İnci and Emine Şule Yazıcı for their discussions and guidance on the theoretical parts of the paper. This project was supported in part by the project METU ADEP-312-2024-11525. Dr. Cinbis is supported by the “Young Scientist Awards Program (BAGEP)” of Science Academy, Türkiye. A. M. Tekalp acknowledges support from the Turkish Academy of Sciences (TUBA), and KUIS AI Center. A. Bilican acknowledges support from the KUIS AI Center for the use of its compute resources.

References

- [1] Armen Aghajanyan, Sonal Gupta, and Luke Zettlemoyer. Intrinsic dimensionality explains the effectiveness of language model fine-tuning. In Chengqing Zong, Fei Xia, Wenjie Li, and Roberto Navigli, editors, *Proceedings of the 59th Annual Meeting of the Association for Computational Linguistics and the 11th International Joint Conference on Natural Language Processing (Volume 1: Long Papers)*, pages 7319–7328, Online, August 2021. Association for Computational Linguistics.
- [2] Alan Ansell, Edoardo Maria Ponti, Anna Korhonen, and Ivan Vulić. Composable sparse fine-tuning for cross-lingual transfer, 2023.
- [3] Alan Ansell, Ivan Vulić, Hannah Sterz, Anna Korhonen, and Edoardo M. Ponti. Scaling sparse fine-tuning to large language models, 2024.
- [4] Klaudia Bałazy, Mohammadreza Banaei, Karl Aberer, and Jacek Tabor. Lora-xs: Low-rank adaptation with extremely small number of parameters. *arXiv preprint arXiv:2405.17604*, 2024.
- [5] Kartikeya Bhardwaj, Nilesh Prasad Pandey, Sweta Priyadarshi, Viswanath Ganapathy, Shreya Kadambi, Rafael Esteves, Shubhankar Borse, Paul Whatmough, Risheek Garrepalli, Mart Van Baalen, Harris Teague, and Markus Nagel. Sparse high rank adapters. In *The Thirty-eighth Annual Conference on Neural Information Processing Systems*, 2024.
- [6] Shubhankar Borse, Shreya Kadambi, Nilesh Prasad Pandey, Kartikeya Bhardwaj, Viswanath Ganapathy, Sweta Priyadarshi, Risheek Garrepalli, Rafael Esteves, Munawar Hayat, and Fatih Porikli. FouRA: Fourier low-rank adaptation. In *The Thirty-eighth Annual Conference on Neural Information Processing Systems*, 2024.
- [7] Arnav Chavan, Zhuang Liu, Deepak Gupta, Eric Xing, and Zhiqiang Shen. One-for-all: Generalized lora for parameter-efficient fine-tuning, 2023.
- [8] Li Deng. The mnist database of handwritten digit images for machine learning research. *IEEE Signal Processing Magazine*, 29(6):141–142, 2012.
- [9] Nicki Skafted Detlefsen, Jiri Borovec, Justus Schock, Ananya Harsh, Teddy Koker, Luca Di Liello, Daniel Stancl, Changsheng Quan, Maxim Grechkin, and William Falcon. Torchmetrics - measuring reproducibility in pytorch. *Journal of Open Source Software*, 7(70):4101, 2 2022. Apache-2.0 License.
- [10] Xinyu Ding, Meiqi Wang, Siyu Liao, and Zhongfeng Wang. Block circulant adapter for large language models. In *International Joint Conference on Artificial Intelligence*, 2025.
- [11] Ali Edalati, Marzieh Tahaei, Ivan Kobyzev, Vahid Partovi Nia, James J. Clark, and Mehdi Rezagholizadeh. Krona: Parameter efficient tuning with kronecker adapter, 2022.
- [12] Abdelrahman Elsayed, Sarim Hashmi, Mohammed Elseiagy, Hu Wang, Mohammad Yaqub, and Ibrahim Almakky. Salt: Singular value adaptation with low-rank transformation, 2025.
- [13] Pál Erdős and Alfréd Rényi. On random matrices. *Publ. Math. Inst. Hungar. Acad. Sci.*, 8:455–461, 1964.
- [14] Alan Frieze and Boris Pittel. Perfect matchings in random graphs with prescribed minimal degree. In Michael Drmota, Philippe Flajolet, Danièle Gardy, and Bernhard Gittenberger, editors, *Mathematics and Computer Science III*, pages 95–132, Basel, 2004. Birkhäuser Basel.

- [15] Ziqi Gao, Qichao Wang, Aochuan Chen, Zijing Liu, Bingzhe Wu, Liang Chen, and Jia Li. Parameter-efficient fine-tuning with discrete fourier transform. In *Forty-first International Conference on Machine Learning*, 2024.
- [16] Demi Guo, Alexander M. Rush, and Yoon Kim. Parameter-efficient transfer learning with diff pruning, 2021.
- [17] Soufiane Hayou, Nikhil Ghosh, and Bin Yu. LoRA+: Efficient low rank adaptation of large models. In *Forty-first International Conference on Machine Learning*, 2024.
- [18] Haoze He, Juncheng B Li, Xuan Jiang, and Heather Miller. SMT: Fine-tuning large language models with sparse matrices. In *The Thirteenth International Conference on Learning Representations*, 2025.
- [19] Suhas G Hegde, Shilpy Kaur, and Aruna Tiwari. Vectorfit : Adaptive singular & bias vector fine-tuning of pre-trained foundation models, 2025.
- [20] Edward J Hu, yelong shen, Phillip Wallis, Zeyuan Allen-Zhu, Yuanzhi Li, Shean Wang, Lu Wang, and Weizhu Chen. LoRA: Low-rank adaptation of large language models. In *International Conference on Learning Representations*, 2022.
- [21] Teng Hu, Jiangning Zhang, Ran Yi, Hongrui Huang, Yabiao Wang, and Lizhuang Ma. SaRA: High-efficient diffusion model fine-tuning with progressive sparse low-rank adaptation. In *The Thirteenth International Conference on Learning Representations*, 2025.
- [22] Weizhong Huang, Yuxin Zhang, Xiawu Zheng, Liuyang, Jing Lin, Yiwu Yao, and Rongrong Ji. Dynamic low-rank sparse adaptation for large language models. In *The Thirteenth International Conference on Learning Representations*, 2025.
- [23] Nam Hyeon-Woo, Moon Ye-Bin, and Tae-Hyun Oh. Fedpara: Low-rank hadamard product for communication-efficient federated learning. In *International Conference on Learning Representations*, 2022.
- [24] Sadeep Jayasumana, Srikumar Ramalingam, Andreas Veit, Daniel Glasner, Ayan Chakrabarti, and Sanjiv Kumar. Rethinking fid: Towards a better evaluation metric for image generation. In *2024 IEEE/CVF Conference on Computer Vision and Pattern Recognition (CVPR)*, pages 9307–9315, 2024.
- [25] Tangyu Jiang, Haodi Wang, and Chun Yuan. Diffora: Enabling parameter-efficient llm fine-tuning via differential low-rank matrix adaptation, 2025.
- [26] Ting Jiang, Shaohan Huang, Shengyue Luo, Zihan Zhang, Haizhen Huang, Furu Wei, Weiwei Deng, Feng Sun, Qi Zhang, Deqing Wang, and Fuzhen Zhuang. MoRA: High-Rank Updating for Parameter-Efficient Fine-Tuning, May 2024. arXiv:2405.12130 [cs].
- [27] Jiale Kang. Bone: Block-affine adaptation of large language models, 2024.
- [28] Diederik P. Kingma and Jimmy Ba. Adam: A method for stochastic optimization. In *Int. Conf. Learning Representation (ICLR)*, 2015.
- [29] Dawid Jan Kopiczko, Tijmen Blankevoort, and Yuki M Asano. VeRA: Vector-based random matrix adaptation. In *The Twelfth International Conference on Learning Representations*, 2024.
- [30] Chunyuan Li, Heerad Farkhoor, Rosanne Liu, and Jason Yosinski. Measuring the intrinsic dimension of objective landscapes. In *International Conference on Learning Representations*, 2018.
- [31] Yang Li, Shaobo Han, and Shihao Ji. VB-loRA: Extreme parameter efficient fine-tuning with vector banks. In *The Thirty-eighth Annual Conference on Neural Information Processing Systems*, 2024.
- [32] Vladislav Lialin, Sherin Muckatira, Namrata Shivagunde, and Anna Rumshisky. ReloRA: High-rank training through low-rank updates. In *The Twelfth International Conference on Learning Representations*, 2024.

- [33] Tsung-Yi Lin, Michael Maire, Serge Belongie, James Hays, Pietro Perona, Deva Ramanan, Piotr Dollár, and C Lawrence Zitnick. Microsoft coco: Common objects in context. In *Computer Vision—ECCV 2014: 13th European Conference, Zurich, Switzerland, September 6–12, 2014, Proceedings, Part V 13*, pages 740–755. Springer, 2014.
- [34] Shih-Yang Liu, Chien-Yi Wang, Hongxu Yin, Pavlo Molchanov, Yu-Chiang Frank Wang, Kwang-Ting Cheng, and Min-Hung Chen. Dora: Weight-decomposed low-rank adaptation. In *ICML*, 2024.
- [35] Weiyang Liu, Zeju Qiu, Yao Feng, Yuliang Xiu, Yuxuan Xue, Longhui Yu, Haiwen Feng, Zhen Liu, Juyeon Heo, Songyou Peng, Yandong Wen, Michael J. Black, Adrian Weller, and Bernhard Schölkopf. Parameter-efficient orthogonal finetuning via butterfly factorization. In *ICLR*, 2024.
- [36] Ilya Loshchilov and Frank Hutter. Decoupled weight decay regularization. In *International Conference on Learning Representations*, 2019.
- [37] Xinyu Ma, Xu Chu, Zhibang Yang, Yang Lin, Xin Gao, and Junfeng Zhao. Parameter efficient quasi-orthogonal fine-tuning via givens rotation. In *Forty-first International Conference on Machine Learning*, 2024.
- [38] Sourab Mangrulkar, Sylvain Gugger, Lysandre Debut, Younes Belkada, Sayak Paul, and Benjamin Bossan. Peft: State-of-the-art parameter-efficient fine-tuning methods. <https://github.com/huggingface/peft>, 2022.
- [39] Van-Anh Nguyen, Thanh-Toan Do, Mehrtash Harandi, Dinh Phung, and Trung Le. Optimizing Specific and Shared Parameters for Efficient Parameter Tuning, April 2025. arXiv:2504.03450 [cs].
- [40] Mahdi Nikdan, Soroush Tabesh, Elvir Crnčević, and Dan Alistarh. RoSA: Accurate parameter-efficient fine-tuning via robust adaptation. In *Forty-first International Conference on Machine Learning*, 2024.
- [41] Maxime Oquab, Timothée Darcet, Théo Moutakanni, Huy V. Vo, Marc Szafraniec, Vasil Khalidov, Pierre Fernandez, Daniel HAZIZA, Francisco Massa, Alaaeldin El-Nouby, Mido Assran, Nicolas Ballas, Wojciech Galuba, Russell Howes, Po-Yao Huang, Shang-Wen Li, Ishan Misra, Michael Rabbat, Vasu Sharma, Gabriel Synnaeve, Hu Xu, Herve Jegou, Julien Mairal, Patrick Labatut, Armand Joulin, and Piotr Bojanowski. DINOv2: Learning robust visual features without supervision. *Transactions on Machine Learning Research*, 2024. Featured Certification.
- [42] Dustin Podell, Zion English, Kyle Lacey, Andreas Blattmann, Tim Dockhorn, Jonas Müller, Joe Penna, and Robin Rombach. SDXL: Improving latent diffusion models for high-resolution image synthesis. In *The Twelfth International Conference on Learning Representations*, 2024.
- [43] Zeju Qiu, Weiyang Liu, Haiwen Feng, Yuxuan Xue, Yao Feng, Zhen Liu, Dan Zhang, Adrian Weller, and Bernhard Schölkopf. Controlling text-to-image diffusion by orthogonal finetuning. In *Thirty-seventh Conference on Neural Information Processing Systems*, 2023.
- [44] Alessio Quercia, Zhuo Cao, Arya Bangun, Richard D. Paul, Abigail Morrison, Ira Assent, and Hanno Schar. 11ora: Summation compression for very low-rank adaptation, 2025.
- [45] Alec Radford, Jong Wook Kim, Chris Hallacy, Aditya Ramesh, Gabriel Goh, Sandhini Agarwal, Girish Sastry, Amanda Askell, Pamela Mishkin, Jack Clark, Gretchen Krueger, and Ilya Sutskever. Learning transferable visual models from natural language supervision. In Marina Meila and Tong Zhang, editors, *Proceedings of the 38th International Conference on Machine Learning*, volume 139 of *Proceedings of Machine Learning Research*, pages 8748–8763. PMLR, 18–24 Jul 2021.
- [46] Robin Rombach, Andreas Blattmann, Dominik Lorenz, Patrick Esser, and Björn Ommer. High-resolution image synthesis with latent diffusion models. In *Proceedings of the IEEE/CVF Conference on Computer Vision and Pattern Recognition (CVPR)*, pages 10684–10695, June 2022.

- [47] Nataniel Ruiz, Yuanzhen Li, Varun Jampani, Yael Pritch, Michael Rubinstein, and Kfir Aberman. Dreambooth: Fine tuning text-to-image diffusion models for subject-driven generation. In *Proceedings of the IEEE/CVF Conference on Computer Vision and Pattern Recognition*, 2023.
- [48] Yiming Shi, Jiwei Wei, Yujia Wu, Ran Ran, Chengwei Sun, Shiyuan He, and Yang Yang. Loldu: Low-rank adaptation via lower-diag-upper decomposition for parameter-efficient fine-tuning, 2024.
- [49] Yi-Lin Sung, Varun Nair, and Colin Raffel. Training neural networks with fixed sparse masks. In A. Beygelzimer, Y. Dauphin, P. Liang, and J. Wortman Vaughan, editors, *Advances in Neural Information Processing Systems*, 2021.
- [50] Patrick von Platen, Suraj Patil, Anton Lozhkov, Pedro Cuenca, Nathan Lambert, Kashif Rasul, Mishig Davaadorj, Dhruv Nair, Sayak Paul, William Berman, Yiyi Xu, Steven Liu, and Thomas Wolf. Diffusers: State-of-the-art diffusion models. <https://github.com/huggingface/diffusers>, 2022.
- [51] Sunghyeon Woo, Sol Namkung, Sunwoo Lee, Inho Jeong, Beomseok Kim, and Dongsuk Jeon. PaCA: Partial connection adaptation for efficient fine-tuning. In *The Thirteenth International Conference on Learning Representations*, 2025.
- [52] SHIH-YING YEH, Yu-Guan Hsieh, Zhidong Gao, Bernard B W Yang, Giyeong Oh, and Yanmin Gong. Navigating text-to-image customization: From lyCORIS fine-tuning to model evaluation. In *The Twelfth International Conference on Learning Representations*, 2024.
- [53] Fangzhao Zhang and Mert Pilanci. Spectral adapter: Fine-tuning in spectral space. In *The Thirty-eighth Annual Conference on Neural Information Processing Systems*, 2024.
- [54] Jia-Chen Zhang, Yu-Jie Xiong, Chun-Ming Xia, Dong-Hai Zhu, and Xi-He Qiu. Parameter-efficient fine-tuning of large language models via deconvolution in subspace. In *Proceedings of the 31st International Conference on Computational Linguistics*, pages 3924–3935. Association for Computational Linguistics, January 2025.
- [55] Juzheng Zhang, Jiacheng You, Ashwinee Panda, and Tom Goldstein. Lori: Reducing cross-task interference in multi-task low-rank adaptation. *arXiv preprint arXiv:2504.07448*, 2025.
- [56] Linhai Zhang, Jialong Wu, Deyu Zhou, and Yulan He. Proper: A progressive learning framework for personalized large language models with group-level adaptation, 2025.
- [57] Qingru Zhang, Minshuo Chen, Alexander Bukharin, Pengcheng He, Yu Cheng, Weizhu Chen, and Tuo Zhao. Adaptive budget allocation for parameter-efficient fine-tuning. In *The Eleventh International Conference on Learning Representations*, 2023.
- [58] Richard Zhang, Phillip Isola, Alexei A Efros, Eli Shechtman, and Oliver Wang. The unreasonable effectiveness of deep features as a perceptual metric. In *CVPR*, 2018.
- [59] Richard Zhang, Phillip Isola, Alexei A. Efros, Eli Shechtman, and Oliver Wang. The unreasonable effectiveness of deep features as a perceptual metric. In *2018 IEEE/CVF Conference on Computer Vision and Pattern Recognition*, pages 586–595, 2018.
- [60] Jiancheng Zhao, Xingda Yu, and Zhen Yang. Msplora: A multi-scale pyramid low-rank adaptation for efficient model fine-tuning, 2025.
- [61] Changhai Zhou, Yuhua Zhou, Qian Qiao, Weizhong Zhang, and Cheng Jin. Efficient fine-tuning of quantized models via adaptive rank and bitwidth. *arXiv preprint arXiv:2505.03802*, 2025.
- [62] Jiacheng Zhu, Kristjan Greenewald, Kimia Nadjahi, Hartz Sáez de Ocariz Borde, Rickard Brüel Gabrielsson, Leshem Choshen, Marzyeh Ghassemi, Mikhail Yurochkin, and Justin Solomon. Asymmetry in low-rank adapters of foundation models. In *ICLR 2024 Workshop on Mathematical and Empirical Understanding of Foundation Models*, 2024.

A Appendix

A.1 Experimental Results and Ablations

This section details our experimental setup, evaluation metrics, main comparison results against state-of-the-art PEFT methods, and ablation studies investigating components of WaveFT and SHiRA [5].

A.1.1 Experimental Setup

Model and Task: All experiments are conducted using the Stable Diffusion XL (SDXL) 1.0 base model [42]. We focus on the task of personalized text-to-image generation, employing the methodology as proposed by DreamBooth [47] and training only the corresponding PEFT adapters while freezing the pretrained weights.

Dataset: We utilize the full set of 30 diverse instances from the DreamBooth benchmark [47] for all main experiments. This dataset encompasses a variety of live subjects and objects. The corresponding real images provided for each instance are used as references for subject fidelity evaluation metrics (DINO, CLIP-I).

Training Details: For each of the 30 instances and every PEFT method evaluated, fine-tuning is applied exclusively to the parameters of the attention layers (specifically, the key, query, value, and output projection matrices within all attention blocks) of the SDXL UNet. The text encoder and all other components of the UNet remain frozen, adhering to common practices for efficient personalization. We employ the AdamW optimizer [36] with a constant learning rate of 1×10^{-4} and train for 500 steps. A per-device batch size of 1 is used, with gradient accumulation over 4 steps, resulting in an effective batch size of 4. All training is performed at the standard SDXL resolution of 1024×1024 pixels.

Parameter Budget: For our main comparisons (Table 3), the number of trainable parameters p for WaveFT and SHiRA [5] is configured to closely match the parameter count of LoRA [20] with rank $r = 1$. For the targeted attention layers in SDXL, this amounts to approximately **1.451 million trainable parameters**. We refer to this configuration as the 'rank-1 equivalent' budget. Parameter counts for all methods are calculated based on the trainable weights within these specified UNet attention layers. For experiments analyzing the effect of varying parameter budgets (e.g., Table 2), p is adjusted accordingly.

We utilize implementations from the Hugging Face PEFT library [38] using their standard configurations where applicable, to ensure reproducibility and fairness. Our WaveFT and SHiRA [5] implementations are designed for compatibility.

Other Hyperparameters: Our proposed method WaveFT and SHiRA [5], by default, utilize zero-initialized trainable parameters, an adapter output scaling factor $\lambda = 25$, and a fixed number of p parameters per adapted layer. For WaveFT, the Daubechies 1 (Haar) wavelet is the default. Experiments were run in bf16 precision with equal parameter budget, with exceptions for LoHA (approx. 2.9M parameters due to its architecture) and FourierFT (fp32 due to library limitations), whose results should be considered in this context.

λ -equivalent parameters for baseline adapters: For all baseline methods, we conducted comprehensive hyperparameter searches to determine optimal configurations that ensure fair comparison. For LoRA [20], following the conventions in diffusers for the SDXL model [50], we set $\alpha = r$ (where r is the rank). For other methods, we determined the following optimal configurations:

- **VeRA:** Learning rate of 3.2×10^{-3} (32 times the base learning rate)
- **AdaLoRA:** $\alpha = 32$
- **LoHA:** $\alpha = 64$
- **FourierFT:** Scaling factor scale = 64
- **LoKR:** $\alpha = 192$

These hyperparameter values were determined through ablation studies to ensure each method performs optimally within its parameter budget constraints. For all methods, we utilized implementa-

tions from the Hugging Face PEFT library [38] with their standard configurations where applicable, modified only by the parameters specified above.

Evaluation Protocol: For each of the 30 instances, we generate 4 images for each of the 25 standard prompts provided by the DreamBooth benchmark [47]. This results in 100 generated images per instance (3000 images per method in total across all instances) for quantitative evaluation. All images are generated using a fixed set of seeds for comparability across methods.

A.1.2 Evaluation Metrics

We assess the performance of each PEFT method using a comprehensive suite of metrics targeting different facets of personalized image generation quality:

- **DINO Score (Subject Fidelity):** Measures the average cosine similarity between DINOv2 [41] ViT-B/14 (facebook/dinov2-base) CLS token embeddings of generated images and the average DINOv2 CLS token embedding of the corresponding real images for the specific instance subject. Higher scores indicate better visual resemblance to the target subject’s identity and key features.
- **CLIP-I Score (Subject Fidelity):** Calculates the average cosine similarity between CLIP ViT-B/32 (openai/clip-vit-base-patch32) image embeddings (pooler output) of generated images and the average CLIP image embedding of the real images for the instance. This offers another perspective on subject fidelity through CLIP’s image feature space. Higher scores are better.
- **CLIP-T Score (Prompt Fidelity):** Computes the average CLIP [45] (using openai/clip-vit-base-patch32) between the generated images and their corresponding input text prompts. This metric evaluates how well the generated image aligns with the textual description. Higher scores indicate better prompt adherence.
- **Diversity (DIV) Score (Intra-Prompt Dissimilarity):** Assesses the diversity of images generated for the same prompt. We calculate the average pairwise Learned Perceptual Image Patch Similarity (LPIPS) [59] (using the TorchMetrics [9] implementation with VGG weights and input normalization) between the 4 images generated for each prompt (resulting in $Comb(4, 2) = 6$ pairs). This is then averaged across all prompts and instances as in [47]. Then this average is subtracted from 1 to measure diversity rather than similarity.
- **CMMD (Distributional Similarity to Real Images):** We compute the CLIP-based Maximum Mean Discrepancy (CMMD) [24] using CLIP ViT-B/32 image embeddings. This metric compares the distribution of embeddings from all 3000 generated images (across all instances and prompts for a given method) against the distribution of embeddings from a large reference set of real images (COCO-30k [33]). **Lower CMMD scores are better**, indicating that the overall distribution of generated images is closer to that of natural images.

For DINO, CLIP-I, CLIP-T, and DIV scores, we report the mean over the 30 instances. Confidence intervals (95%) are provided for all metrics, calculated via bootstrapping with 10,000 iterations over the 30 instances.

A.1.3 Computational Complexity

All of the experiments above are done in 46gb NVIDIA A40 GPU’s. LoRA takes around 20 minutes to train for a single instance, SHiRA [5] also takes around 22 minutes and WaveFT takes about 34 minutes.

A significant advantage of WaveFT which is shared with LoRA [20], is their inference efficiency. Once trained, the learned adapter update ΔW can be merged with the base model weights W_0 , thereby incurring no additional computational latency during inference compared to the original model, as discussed in Section 3.

During training, SHiRA [5] is computationally efficient as it only requires updating p sparse parameters directly in the coefficient matrix C and involves sparse matrix operations. WaveFT introduces an additional computational step compared to SHiRA [5] due to the Inverse Discrete Wavelet Transform (IDWT) applied to the sparse coefficient matrix C to form ΔW_{WaveFT} , and the corresponding Discrete Wavelet Transform (DWT) in the backward pass for gradient computation. The complexity of these

transforms depends on the chosen wavelet (e.g., Daubechies 1/Haar) and implementation, but is typically efficient, especially considering that C is sparse.

It is important to note that all these PEFT methods—WaveFT, SHiRA [5], and LoRA [20]—offer substantial reductions in both the number of trainable parameters and overall training time compared to full fine-tuning of the large-scale SDXL model.

In summary, while WaveFT incurs a modest computational overhead during training compared to the direct sparse updates of SHiRA [5] due to the wavelet transforms, but WaveFT maintains the crucial advantage of zero latency overhead at inference time.

A.2 MNIST Classification 6

To evaluate the versatility of WaveFT and SHiRA [5] beyond complex generative models, we conducted a comparative analysis on the MNIST handwritten digit classification task. This experiment provides insights into the effectiveness of these methods in a simpler, well-understood domain and demonstrates their potential as general-purpose parameter-efficient layers.

Experimental Setup. We implemented a simplified single-layer architecture for the MNIST classification task where each method (LoRA [20], SHiRA [5], and WaveFT) was used as the sole trainable component connecting the flattened input images (784 dimensions) to the output classes (10 dimensions). This controlled setting allowed for a direct comparison of the representational capacity and parameter efficiency of each approach.

The experiments were conducted using the standard MNIST dataset [8] (60,000 training images, 10,000 test images). We used a batch size of 64, the Adam optimizer [28] with an initial learning rate of 0.01, and a step scheduler with $\gamma = 0.5$ and step size of 5 epochs. All models were trained for 50 epochs using cross-entropy loss.

For each method, we varied the parameter budget systematically to evaluate the performance scaling. LoRA [20] was tested with ranks $r \in \{1, 2, 3, 4, 5, 6\}$. SHiRA [5] and WaveFT were tested with parameter counts either equivalent to LoRA configurations or below LoRA’s minimum rank ($r = 1$), a key advantage of our sparse parameterization approach. The trainable parameters were randomly selected within the weight matrix for SHiRA [5], while for WaveFT, the inverse discrete wavelet transform was applied to the weight matrix using the Haar/Debauchies 1 wavelets.

Performance Evaluation. Classification accuracy on the test set was used as the primary evaluation metric. We recorded performance for each method across various parameter budgets to plot the accuracy-vs-parameters curve shown in Figure 8.

The MNIST experiments provided valuable evidence that both SHiRA [5] and WaveFT can function effectively as standalone classification layers with very few parameters. As shown in Figure 8, our proposed methods achieved superior accuracy compared to LoRA [20], particularly in the extremely parameter-constrained regimes. This demonstrates that the approaches developed for fine-tuning large generative models can also be applied effectively in simpler discriminative tasks, suggesting broader applicability across various machine learning domains.

A.3 Empirical Demonstration of Block-Sparse Interpolation Capacity

To illustrate the practical implications of Lemma 3, we conducted an experiment involving mapping $k = 5$ random input vectors to $k = 5$ random output vectors in a high-dimensional space. This setup creates a representative interpolation problem that aligns with the conditions in Lemma 3, where we set the dimensionality to 784×784 and tested varying numbers of trainable parameters.

Experimental Setup. We implemented a sparse matrix model (SHiRA [5]) which constructs a weight matrix with trainable parameters randomly selected from the total 784^2 possible positions. The model was trained to map 5 random input vectors of dimension 784 to 5 random output vectors of the same dimension, all sampled from a normal distribution. The remaining elements were fixed at zero throughout training.

We used the Mean Squared Error (MSE) as the loss function and Adam optimizer [28] with an initial learning rate of 0.01. A step scheduler reduced the learning rate by a factor of $\gamma = 0.75$ every 500

epochs. The model was trained for a total of 5,000 epochs to ensure convergence. We systematically varied the number of trainable parameters to determine the minimum count required for successful interpolation.

Performance Evaluation. The empirical results shown in Figure 7 strongly support our theoretical analysis. At approximately 15,680 trainable parameters, the training loss converges to zero with high confidence, demonstrating that the sparse model successfully learns to map the input vectors to their target outputs with high precision.

This confirms that when sufficient trainable parameters are appropriately distributed through random selection, the sparse matrix can perfectly interpolate between arbitrary input-output pairs, validating the practical implications of Lemma 3. This result is particularly relevant for understanding the effectiveness of SHiRA [5], which leverages sparse parameterization to achieve high representational capacity with a small number of trainable parameters.

A.4 Proofs

Lemma (Subspace Bottleneck of LoRA). *For a rank- r adapter update matrix of the form $\Delta W = BA^\top$, where $B \in \mathbb{R}^{m \times r}$ and $A \in \mathbb{R}^{n \times r}$, the following properties hold:*

1. *The image (column space) of ΔW is contained within the span of the columns of B :*

$$\text{im}(\Delta W) = \{\Delta W x \mid x \in \mathbb{R}^n\} \subseteq \text{span}(\text{columns of } B).$$

2. *The kernel (null space) of ΔW contains the orthogonal complement of the span of the columns of A :*

$$\ker(\Delta W) = \{x \in \mathbb{R}^n \mid \Delta W x = 0\} \supseteq (\text{span}(\text{columns of } A))^\perp = \ker(A^\top).$$

Consequently, any update ΔW achieved through such a factorization can only modify the network's activations within the r -dimensional subspace spanned by the columns of B . Directions orthogonal to the columns of A in the input space are mapped to zero.

Proof. 1. For any x , $\Delta W x = B(A^\top x)$ is a linear combination of B 's columns, so $\text{im}(\Delta W) \subseteq \text{span}(B)$. 2. If $x \in \ker(A^\top)$ then $A^\top x = 0$, so $\Delta W x = B0 = 0$, hence $\ker(A^\top) \subseteq \ker(\Delta W)$. This completes the proof of the bottleneck. \square

Lemma (Block-Sparse Interpolation Capacity). *Let $W_0 \in \mathbb{R}^{m \times n}$ be any fixed matrix. Let*

$$\{x^{(1)}, \dots, x^{(k)}\} \subset \mathbb{R}^n$$

be linearly independent, and let arbitrary targets $\{y^{(1)}, \dots, y^{(k)}\} \subset \mathbb{R}^m$ be given. Set

$$X = [x^{(1)} \dots x^{(k)}] \in \mathbb{R}^{n \times k}, \quad Z = [y^{(1)} - W_0 x^{(1)} \dots y^{(k)} - W_0 x^{(k)}] \in \mathbb{R}^{m \times k}.$$

Let $S \subset [m] \times [n]$ be a fixed sparse support pattern, and define

$$R = \{i \in [m] \mid Z_{i,:} \neq 0\}, \quad S_i = \{j \in [n] \mid (i, j) \in S\}.$$

Assume:

1. $\text{rank}(X) = k$.
2. *There exists a single index set*

$$C = \{c_1, \dots, c_k\} \subset [n]$$

such that $X_{C,:} \in \mathbb{R}^{k \times k}$ is invertible and $C \subset S_i$ for every $i \in R$.

Then one can construct $\Delta W \in \mathbb{R}^{m \times n}$ with

1. $\text{supp}(\Delta W) \subseteq S$.
2. $(W_0 + \Delta W)x^{(l)} = y^{(l)}$ for all $l = 1, \dots, k$.

3. $\text{rank}(\Delta W) = \text{rank}(Z_R)$, where Z_R is the submatrix of Z restricted to rows in R .

Proof. Step 1: Existence of an invertible block. Since $\text{rank}(X) = k$, there exists at least one k -subset $C \subset [n]$ for which the submatrix $X_{C,:}$ is nonsingular. By hypothesis (2), we choose such a C and furthermore have $C \subset S_i$ for every $i \in R$.

Step 2: Construction of ΔW . Define ΔW row-wise by

$$(\Delta W)_{i,j} = \begin{cases} (Z_{i,:} (X_{C,:})^{-1})_r, & i \in R, j = c_r \in C, \\ 0, & \text{otherwise.} \end{cases}$$

Equivalently, for each $i \in R$ the row $(\Delta W)_{i,:}$ has its only potentially nonzero entries in columns C , given by the $1 \times k$ vector $Z_{i,:} (X_{C,:})^{-1}$. For $i \notin R$, set the i -th row to zero.

Step 3: Verification of properties.

(i) *Sparsity.* By construction, the only nonzero entries of row $i \in R$ lie in columns $C \subset S_i$, and rows $i \notin R$ are entirely zero. Hence $\text{supp}(\Delta W) \subseteq S$.

(ii) *Exact interpolation $\Delta W X = Z$.* Fix any row i :

- If $i \notin R$, then $Z_{i,:} = 0$ and $(\Delta W)_{i,:} = 0$, so $(\Delta W)_{i,:} X = 0 = Z_{i,:}$.
- If $i \in R$, only columns in C contribute:

$$(\Delta W)_{i,:} X = (Z_{i,:} (X_{C,:})^{-1}) X_{C,:} = Z_{i,:},$$

since $X_{C,:}$ is invertible. Thus $\Delta W X = Z$, and $(W_0 + \Delta W)x^{(l)} = W_0 x^{(l)} + Z_{:,l} = y^{(l)}$ for each l .

(iii) *Rank lower bound.* Let ΔW_R and Z_R be the submatrices restricted to rows in R . Observe that $\Delta W_R = Z_R (X_{C,:})^{-1} E$, where $E \in \mathbb{R}^{k \times n}$ is the embedding that places the k columns into positions C . Note:

$$\text{rank}(\Delta W_R) = \text{rank}(Z_R (X_{C,:})^{-1} E) = \text{rank}(Z_R),$$

because left-multiplication by the invertible $(X_{C,:})^{-1}$ and the column-embedding E both preserve the row-rank. Rows outside R of ΔW are zero, so $\text{rank}(\Delta W) = \text{rank}(\Delta W_R) = \text{rank}(Z_R)$.

This completes the proof. □

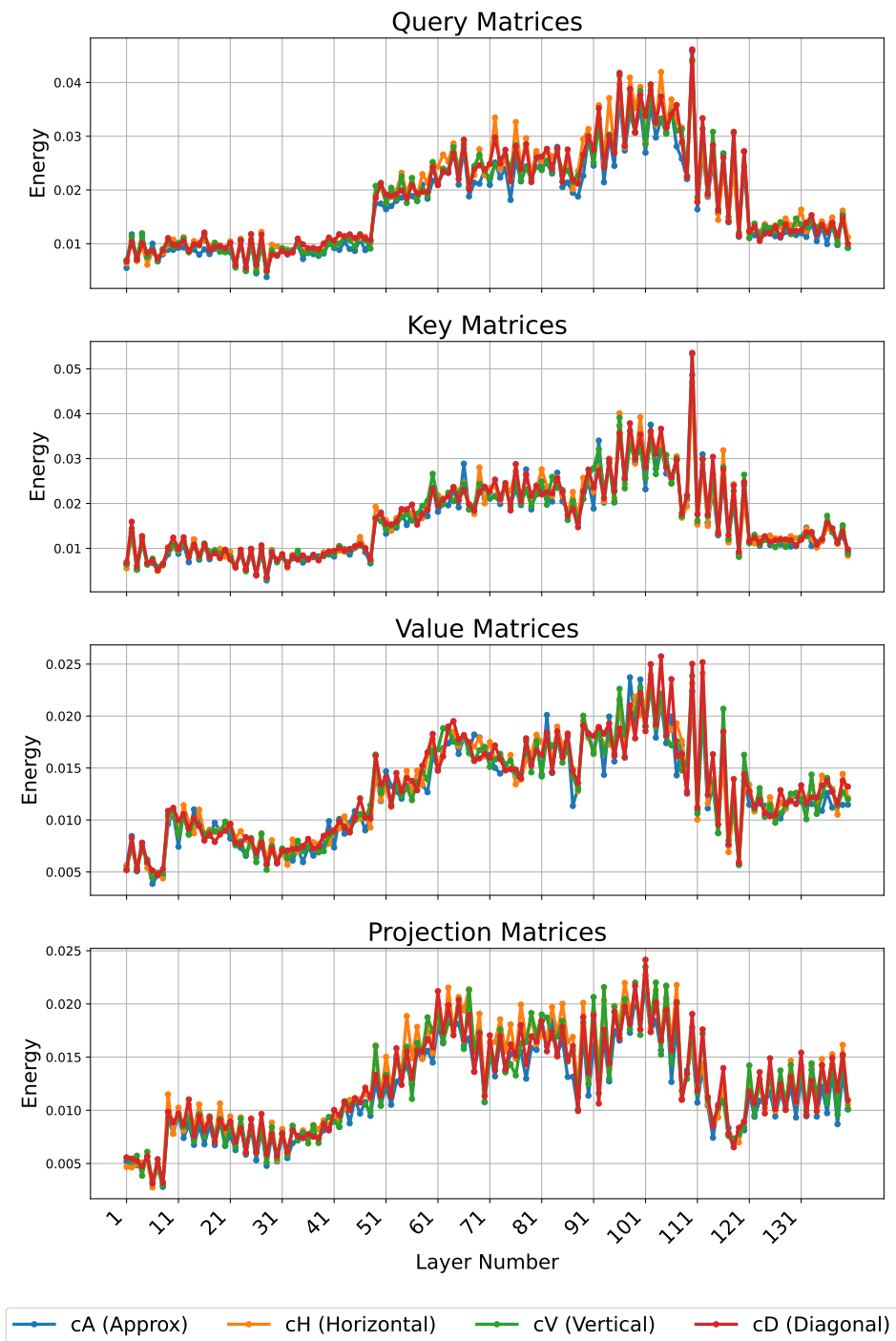


Figure 9: The energy distribution of wavelet coefficients throughout layers

A.5 Tables

Table 1: Evaluation Summary for Wavelet Families (Coiflet, Symlet, Debauchies) Ordered by Name. Confidence intervals are shown below the mean value as [-lower difference, +upper difference].

Configuration Name	DINO Sim \uparrow	CLIP-I Sim \uparrow	CLIP-T Score \uparrow	LPIPS Diversity \uparrow	CMMD Value \downarrow
Debauchies 1	0.4950 [-0.0079, +0.0080]	0.6545 [-0.0043, +0.0043]	32.4121 [-0.1317, +0.1339]	0.3475 [-0.0030, +0.0029]	1.265
Debauchies 2	0.4942 [-0.0081, +0.0076]	0.6544 [-0.0042, +0.0042]	32.3726 [-0.1312, +0.1297]	0.3420 [-0.0030, +0.0029]	1.300
Debauchies 3	0.4930 [-0.0082, +0.0078]	0.6531 [-0.0043, +0.0043]	32.4174 [-0.1343, +0.1361]	0.3433 [-0.0029, +0.0030]	1.312
Coiflet 1	0.4893 [-0.0077, +0.0079]	0.6513 [-0.0041, +0.0041]	32.2810 [-0.1329, +0.1352]	0.3422 [-0.0029, +0.0029]	1.279
Coiflet 2	0.4926 [-0.0079, +0.0079]	0.6546 [-0.0044, +0.0043]	32.2956 [-0.1339, +0.1358]	0.3456 [-0.0029, +0.0028]	1.306
Symlet 2	0.4930 [-0.0078, +0.0079]	0.6547 [-0.0044, +0.0042]	32.3512 [-0.1349, +0.1335]	0.3422 [-0.0030, +0.0030]	1.303
Symlet 3	0.4950 [-0.0077, +0.0079]	0.6548 [-0.0044, +0.0041]	32.3891 [-0.1347, +0.1351]	0.3453 [-0.0029, +0.0030]	1.321
Symlet 4	0.4938 [-0.0081, +0.0078]	0.6534 [-0.0041, +0.0043]	32.3615 [-0.1369, +0.1328]	0.3463 [-0.0031, +0.0029]	1.278

Table 2: Evaluation Summary for LoRA, SHiRA, and WaveFT Configurations Sorted by Rank. Confidence intervals are shown below the mean value as [-lower difference, +upper difference].

Configuration Name	DINO Sim \uparrow	CLIP-I Sim \uparrow	CLIP-T Score \uparrow	LPIPS Diversity \uparrow	CMMD Value \downarrow
WaveFT (rank=0.8)	0.4685 [-0.0076, +0.0077]	0.6418 [-0.0042, +0.0041]	32.4637 [-0.1333, +0.1290]	0.3339 [-0.0028, +0.0028]	1.265
SHiRA (rank=0.8)	0.4401 [-0.0075, +0.0074]	0.6320 [-0.0041, +0.0042]	32.1286 [-0.1387, +0.1348]	0.3365 [-0.0029, +0.0028]	1.265
SHiRA (rank=0.9)	0.4512 [-0.0076, +0.0075]	0.6389 [-0.0043, +0.0041]	32.1140 [-0.1368, +0.1399]	0.3397 [-0.0029, +0.0030]	1.273
WaveFT (rank=0.9)	0.4780 [-0.0078, +0.0077]	0.6449 [-0.0043, +0.0042]	32.4744 [-0.1369, +0.1315]	0.3412 [-0.0030, +0.0030]	1.236
LoRA	0.4628 [-0.0077, +0.0075]	0.6400 [-0.0042, +0.0041]	32.3946 [-0.1334, +0.1336]	0.3085 [-0.0028, +0.0029]	1.275
SHiRA	0.4673 [-0.0079, +0.0078]	0.6451 [-0.0041, +0.0041]	32.0934 [-0.1343, +0.1350]	0.3417 [-0.0029, +0.0029]	1.254
WaveFT	0.4950 [-0.0079, +0.0080]	0.6545 [-0.0043, +0.0043]	32.4121 [-0.1317, +0.1339]	0.3475 [-0.0030, +0.0029]	1.265
SHiRA (rank=1.5)	0.5322 [-0.0077, +0.0076]	0.6744 [-0.0041, +0.0040]	31.9234 [-0.1384, +0.1375]	0.3610 [-0.0031, +0.0031]	1.283
WaveFT (rank=1.5)	0.5317 [-0.0082, +0.0080]	0.6734 [-0.0043, +0.0042]	32.0445 [-0.1382, +0.1356]	0.3598 [-0.0031, +0.0031]	1.247
LoRA (rank=2)	0.4974 [-0.0075, +0.0075]	0.6553 [-0.0040, +0.0040]	32.2320 [-0.1357, +0.1330]	0.3150 [-0.0029, +0.0029]	1.298
SHiRA (rank=2)	0.5673 [-0.0076, +0.0076]	0.6918 [-0.0039, +0.0039]	31.7078 [-0.1425, +0.1375]	0.3790 [-0.0031, +0.0032]	1.282
WaveFT (rank=2)	0.5570 [-0.0078, +0.0077]	0.6881 [-0.0042, +0.0042]	31.6796 [-0.1334, +0.1361]	0.3730 [-0.0029, +0.0030]	1.284
LoRA (rank=3)	0.5078 [-0.0075, +0.0078]	0.6622 [-0.0041, +0.0040]	32.1163 [-0.1379, +0.1364]	0.3207 [-0.0030, +0.0030]	1.294
SHiRA (rank=3)	0.6004 [-0.0075, +0.0072]	0.7078 [-0.0039, +0.0038]	31.1268 [-0.1396, +0.1384]	0.3938 [-0.0030, +0.0030]	1.309
WaveFT (rank=3)	0.5988 [-0.0073, +0.0072]	0.7041 [-0.0039, +0.0039]	31.2469 [-0.1350, +0.1362]	0.3875 [-0.0029, +0.0030]	1.313

Table 3: Evaluation Summary for Ablations on WaveFT. Confidence intervals are shown below the mean value as [-lower difference, +upper difference].

Configuration Name	DINO Sim \uparrow	CLIP-I Sim \uparrow	CLIP-T Score \uparrow	LPIPS Diversity \uparrow	CMMD Value \downarrow
Base Version	0.4950 [-0.0079, +0.0080]	0.6545 [-0.0043, +0.0043]	32.4121 [-0.1317, +0.1339]	0.3475 [-0.0030, +0.0029]	1.265
Proportional Parameter Allocation	0.4729 [-0.0079, +0.0076]	0.6436 [-0.0042, +0.0042]	32.4038 [-0.1365, +0.1341]	0.3302 [-0.0029, +0.0028]	1.255
Permutated Input Embedding Experiment	0.4871 [-0.0080, +0.0078]	0.6519 [-0.0042, +0.0041]	32.2815 [-0.1325, +0.1277]	0.3440 [-0.0030, +0.0030]	1.271
Gaussian Initialization	0.0130 [-0.0014, +0.0013]	0.3315 [-0.0017, +0.0016]	20.1346 [-0.0923, +0.0931]	0.3962 [-0.0013, +0.0013]	3.707

Table 4: Evaluation Summary for Different Methods with 95% CIs. Confidence intervals are shown below the mean value as [-lower difference, +upper difference].

Configuration Name	DINO Sim \uparrow	CLIP-I Sim \uparrow	CLIP-T Score \uparrow	LPIPS Diversity \uparrow	CMMD Value \downarrow
LoRA	0.4628 [-0.0077, +0.0075]	0.6400 [-0.0042, +0.0041]	32.3946 [-0.1334, +0.1336]	0.3085 [-0.0028, +0.0029]	1.275
SHiRA	0.4673 [-0.0079, +0.0078]	0.6451 [-0.0041, +0.0041]	32.0934 [-0.1343, +0.1350]	0.3417 [-0.0029, +0.0029]	1.254
WaveFT	0.4950 [-0.0079, +0.0080]	0.6545 [-0.0043, +0.0043]	32.4121 [-0.1317, +0.1339]	0.3475 [-0.0030, +0.0029]	1.265
VeRA	0.4889 [-0.0075, +0.0078]	0.6496 [-0.0043, +0.0041]	32.4818 [-0.1315, +0.1336]	0.3246 [-0.0029, +0.0028]	1.309
AdaLora	0.4676 [-0.0075, +0.0076]	0.6422 [-0.0042, +0.0042]	32.3355 [-0.1300, +0.1303]	0.3059 [-0.0027, +0.0028]	1.274
LoHA	0.4244 [-0.0073, +0.0072]	0.6232 [-0.0041, +0.0041]	32.1687 [-0.1364, +0.1349]	0.3009 [-0.0027, +0.0028]	1.268
FourierFT	0.2153 [-0.0066, +0.0065]	0.5184 [-0.0041, +0.0042]	32.3188 [-0.1388, +0.1402]	0.2495 [-0.0026, +0.0027]	1.173
LoKR	0.4493 [-0.0079, +0.0076]	0.6323 [-0.0042, +0.0044]	32.5345 [-0.1336, +0.1333]	0.3119 [-0.0029, +0.0029]	1.312

Table 5: Sample Variances of Metrics Across Seeds (0-9) for Configuration Groups for the dog instance for LoRA $r = 1$ budget.

Configuration Group	Var (DINO Sim)	Var (CLIP-I Sim)	Var (CLIP-T Score)	Var (LPIPS Diversity)	Var (CMMD Value)
SHiRA	0.00105251	0.00009462	0.05590719	0.99972289	0.01821341
WaveFT	0.00080235	0.00008035	0.03283789	0.99991386	0.03002796

Table 6: Evaluation Summary for Different λ values for LoRA rank=4 equivalent paramter budget with 95% CIs. Confidence intervals are shown below the mean value as [-lower difference, +upper difference].

Configuration Name	DINO Sim \uparrow	CLIP-I Sim \uparrow	CLIP-T Score \uparrow	LPIPS Diversity \uparrow	CMMD Value \downarrow
WaveFT $\lambda=5$	0.4738 [-0.0079, +0.0078]	0.6430 [-0.0042, +0.0043]	32.5657 [-0.1334, +0.1316]	0.3350 [-0.0029, +0.0030]	1.330
WaveFT $\lambda=10$	0.5471 [-0.0080, +0.0078]	0.6803 [-0.0042, +0.0042]	31.9829 [-0.1320, +0.1343]	0.3641 [-0.0031, +0.0031]	1.327
WaveFT $\lambda=15$	0.5884 [-0.0075, +0.0075]	0.7024 [-0.0039, +0.0039]	31.5831 [-0.1357, +0.1389]	0.3853 [-0.0032, +0.0031]	1.293
WaveFT $\lambda=20$	0.6211 [-0.0070, +0.0070]	0.7196 [-0.0036, +0.0037]	31.0686 [-0.1394, +0.1377]	0.3905 [-0.0031, +0.0029]	1.299
WaveFT $\lambda=25$	0.6267 [-0.0065, +0.0066]	0.7131 [-0.0035, +0.0035]	30.3889 [-0.1358, +0.1359]	0.3865 [-0.0027, +0.0025]	1.417